Journal of Advanced Research in Fluid Mechanics and Thermal Sciences

Journal homepage:
https://semarakilmu.com.my/journals/index.php/fluid_mechanics_thermal_sciences/index
ISSN: 2289-7879

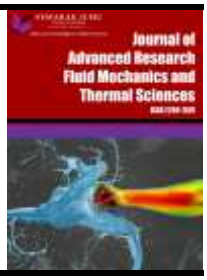

The Analytical Improvement of q-Homotopy Analysis Method for Magneto-hydrodynamic (MHD) Jeffrey Hamel Nanofluid Flow

Haedir Abd AlRazak Namoos[1,*], Abeer Majeed Jasim[1]

[1] Department of Mathematics, College of Science, University of Basrah, Basrah, Iraq

ARTICLE INFO

Article history:
Received 25 March 2024
Received in revised form 22 June 2024
Accepted 5 July 2024
Available online 30 July 2024

Keywords:
q-homotopy analysis method; Laplace transform; EL-Zaki transform; convolution theory; Jeffrey-Hamel flow; magneto-hydrodynamic; nanoparticle

ABSTRACT

The present study analyzes the velocity distribution for magneto-hydrodynamic (MHD) Jeffrey Hamel nanofluid with nanoparticles between two non-parallel planar walls divergent and convergent channels the governing equations for this problem are reduced to an ordinary differential equation. This is demonstrated through the use of a new analytical method called q-homotopy analysis (q-HAM). This new technique is based on combining the q-HAM method with the Laplace transform (LT) and the EL-Zaki transform (ZT) in the presence of convolution theory in this research. The results proved that the improved solutions obtained from this problem were proven to be highly accurate by comparing them using Bvp4c, a Maple built-in function. As wall as the impact of emerging parameters such as Reynolds number, Hartmann number and open angle is discussed for three material Al_2O_3, TiO_2 and Cu. The results show that the increment in velocity distribution occurs through growing Hartmann number for both channels, While the opposite of the case occurs, which shows a reduce in the velocity distribution with a rise in the Reynolds number.

1. Introduction

The motion of nanofluids, which are engineered colloidal suspensions made up of a base fluid (like water, oil, or ethylene glycol) and nanoparticles that are usually between one and hundred nanometers in size, is referred to as nanofluid flow. The high surface area to volume ratio of nanoparticles and their molecular interactions with the base fluid give rise to the special characteristics of nanofluids. When compared to traditional fluids, these properties may improve rheological behavior, heat transfer, and other fluid dynamic properties. Nanofluid flow finds use in a number of areas, such as oil recovery procedures, electronic device cooling, biomedical applications, and thermal systems with improved heat transfer. To maximize their performance and create effective systems, designers must have a thorough understanding of how nanofluids behave under flow conditions [1-3]. These nanoparticles are frequently found in nature as non-metallic and metallic materials can be described in Figure 1 as follows

* *Corresponding author.*
E-mail address: haedirnamoos@gmail.com

https://doi.org/10.37934/arfmts.119.2.3255

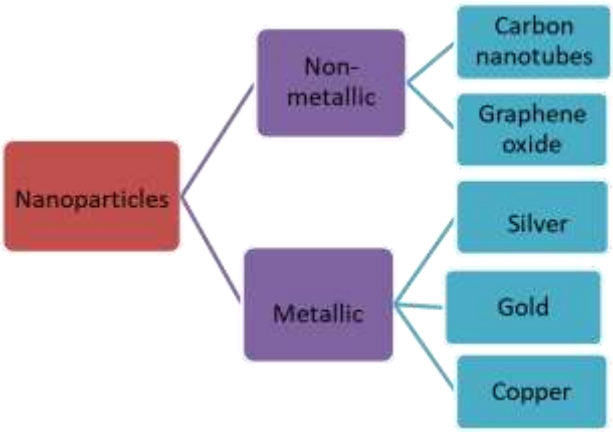

Fig. 1. The materials of nanoparticles

When constrained fluid flow between two inclined parallel plates is considered, the resulting flow is known as Jeffrey Hamel flow. In incompressible viscous fluid flow through converging and diverging channels, Jeffrey [4] and Hamel *et al.,* [5], the complex fluid flow phenomenon is represented by the magneto-hydrodynamic (MHD) flow system Jeffrey Hamel indicates a continuous and incompressible flow in an expanding two-dimensional channel or gradually shrink in one direction. The electrically conducting fluid in this case would be liquid metal. In order to account for the effects of the magnetic field, this flow configuration is frequently modeled using a combination of Maxwell's equations and the Navier-Stokes equations. Despite its importance, the complicated connection between fluid dynamics and electromagnetic makes Jeffrey-Hamel flow difficult to theoretically understand, numerically simulate, and empirically confirm. Research is still being done in order to better comprehend MHD flows, produce more exact modeling approaches, and examine novel applications in emerging technology. More research has been done in order to better comprehend MHD flows, develop more precise modeling approaches, and study potential applications in emerging technologies. As a result, researchers can acquire helpful understanding into the interplay between fluid flow, magnetic fields, and the dynamics of nanoparticles inside the system [1,5-9]. The quest for analytical solutions, however, remains crucial since they help us understand the system's fundamental dynamics and provide significant fresh views on how the system operates. Understanding complex physical processes requires the use of approximate analytical solutions, which provide simple and intuitive descriptions of the fundamental dynamics. An approximate analytical solution is a mathematical formula or statement that describes a system's behavior under specific simplification hypotheses. These solutions simplify analysis and interpretation by emphasizing the most significant components of the issue while omitting the less important ones. When obtaining perfect solutions is difficult or impossible, approximate analytical solutions might help. They can serve as benchmarks for experimentation or numerical simulations, providing useful information about how a system operates. Although due to the simplification hypotheses, its usefulness is typically limited to certain regimes or parameter ranges. In this study, we use the q-homotopy analysis method to solve nonlinear differential equations without the need for a perturbation parameter. The objective of the present work is to improve the q-homotopy analysis method and investigate the effect of the angles between the plates, Reynold number, magnetic number, and nanoparticles volume fraction on the velocity profile by using some transformations such as the Laplace transform and the El-Zaki transform that we see in previous works supported by convolution theory as our guide when we propose a new analytical technique to overcome the numerical problems that appear in some prioritization methods [10-14]. Furthermore, it proposes a new analytical method through which we can overcome the numerical difficulties that appear in

some previous methods. According to our limited knowledge and previous research, it has been shown that the use of approximate analytical methods combined with integral transformations may significantly reduce many difficulties. To show the applicability, validity, and accuracy of this method, we have compared it with LTC-q-HAM, ETC-q-HAM, and the numerical method bvp4c in diagrams and tables. The basic properties of nano-fluid and nanoparticles can be listed in the following Table 1:

Table 1
Properties of nano-fluid and nanoparticles

Material	$\rho(kg/m^3)$	$CP(J/kgk)$	$k(W/mk)$
Al_2O_3	3970	765	40
TiO_2	4250	686.2	8.9538
Cu	8933	385	401
Fluid phase (water)	997.1	4179	0.613

2. The Problem Statement

The physics problem of Jeffery Hamel describes a two-dimensional flowing incompressible nanoparticle under consideration that conducts viscous fluid from a source or sink at the junction between two rigid plane walls whose angle is 2φ as shown in Figure 2. In general, the flow depends on r and θ that is the magnetic field acts transversely with the flow. The governing equations are defined mathematically in polar coordinates as follows [15,16]

$$\frac{\hat{\rho}_{nf}}{r}\frac{\partial(ru)}{\partial r} = 0, \tag{1}$$

$$u\frac{\partial u}{\partial r} + \frac{1}{\hat{\rho}_{nf}}\frac{\partial \tilde{p}}{\partial r} - \vartheta_{nf}\left[\frac{\partial^2 u}{\partial r^2} + \frac{1}{r}\frac{\partial u}{\partial r} + \frac{1}{r^2}\frac{\partial^2 u}{\partial r^2} - \frac{u}{r^2}\right] + \frac{\sigma C_0^2}{\hat{\rho}_{nf}}u = 0, \tag{2}$$

$$\frac{1}{\hat{\rho}_{nf}r}\frac{\partial \tilde{p}}{\partial \theta} - \frac{2\vartheta_{nf}}{r^2}\frac{\partial u}{\partial \theta} = 0, \tag{3}$$

where C_0 electromagnetic induction, $\tilde{p}$ is the fluid pressure, u is the velocity along the radial direction, σ the conductivity of the fluid, $\hat{\rho}$ the fluid density, and ϑ the coefficient of kinematic viscosity. The nano-fluid are given as

$$\hat{\rho}_{nf} = \hat{\rho}_f(1-w) + \hat{\rho}_s w,\ \breve{\mu}_{nf} = \frac{\breve{\mu}_f}{(1-w)^{2.5}},\ \vartheta_{nf} = \frac{\breve{\mu}_f}{\hat{\rho}_{nf}}, \tag{4}$$

Here, w is the solid volume fraction. Also, by integrating both sides concerning r of Eq. (1), yield

$$\bar{f}(\theta) = ru(r,\theta), \tag{5}$$

From Eq. (5) the dimensionless form of the velocity parameter can be obtained by dividing that by its maximum value as follows

$$\bar{f}\,(\tau) = \frac{\bar{f}(\theta)}{\bar{f}_{max}},\ \ \tau = \frac{\theta}{\varphi}, \tag{6}$$

where φ is the semi-angle between the two inclined walls. The resulting nonlinear ordinary differential equation after eliminating the pressure value $\tilde{p}$ by differentiating Eq. (2) and Eq. (3) concerning θ and r respectively with the dimensionless variables in Eq. (6), is displayed as follows:

$$\frac{d^3\bar{f}}{d\tau^3} + 2\varphi Re((1-w) + \frac{\hat{\rho}_s}{\hat{\rho}_f}w)(1-w)^{2.5}\bar{f}\frac{d\bar{f}}{d\tau} + (4-(1-w)^{1.25}Ha)\varphi^2\frac{d\bar{f}}{d\tau} = 0, \tag{7}$$

with the boundary conductions

$$\bar{f}\,(0) = 1, \quad \frac{d\bar{f}(0)}{d\tau} = 0, \bar{f}\,(1) = 0, \tag{8}$$

The Reynolds number and the Hartmann number can be introduced by

$$Re = \frac{\bar{f}_{max}\varphi}{\vartheta}\begin{pmatrix} divergent\ channel: \varphi > 0, \bar{f}_{max} > 0 \\ convergent\ channel: \varphi < 0, \bar{f}_{max} < 0 \end{pmatrix}, Ha = \sqrt{\frac{\sigma C_0^2}{\hat{\rho}\vartheta}}, \tag{9}$$

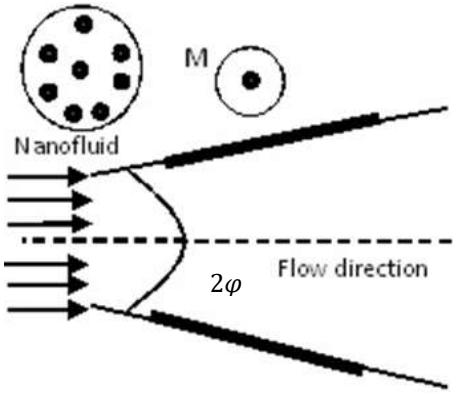

Fig. 2. Schematic of the problem

3. Fundamental Ideal of q- Homotopy Analysis Method

q-Homotopy Analysis is a method based on the standard perturbation and homotopy in topology. This approach produces a power series solution that is close to the exact solution. To illustrate the basic concepts of q-HAM, the non-linear differential equation can be represented as follows:

$$D(\bar{f}) + U(\bar{f}) + N(\bar{f}) - g(\tau) = 0, \ \ \tau \in \Omega \qquad \mathcal{K}(\bar{f}(\tau), \frac{d\bar{f}}{d\tau}) = 0\ ; \tau \in \Gamma, \tag{10}$$

where $\bar{f}$ denotes the unknown function, $g(\tau)$ is a known analytic function, $\mathcal{K}$ denote the boundary operator. The boundaries of the field Ω is displayed by Γ. D, U refer to the linear differential operator such that its order is less than D, N the general non-linear differential operator. The definition of the homotopy in the homotopy perturbation technique is $\bar{f}: \mathbb{R} \times [0, \frac{1}{n}] \to \mathbb{R}$ and constructed as

$$H(\bar{f}, q) = (1-nq)[D(\bar{f}(\tau, q)) - D(\bar{f}_0)] - qhH(\tau)[D(\bar{f}(\tau)) + U(\bar{f}(\tau)) + N(\bar{f}(\tau)) - g(\tau)] = 0, \tag{11}$$

where D is an appropriate auxiliary linear operator, $q \in [0, \frac{1}{n}], n \geq 1$ denotes the so-called embedded parameter, $H(\tau)$ denotes anon-zero auxiliary function, $h \neq 0$ is an auxiliary parameter and $\bar{f}_0$ is an initial approximation of Eq. (10) that perfectly satisfies the boundary conditions. The general form of the Eq. (11) when substituting for $q = 0,\ q = \frac{1}{n}$ an $H(\tau) = 1$ as the following

$$H(\bar{f}, 0) = D\left(\bar{f}(\tau, 0)\right) - D(\bar{f}_0), \tag{12}$$

$$H\left(\bar{f}, \frac{1}{n}\right) = \frac{h}{n}[D(\bar{f}(\tau, \frac{1}{n}) + U(\bar{f}(\tau, \frac{1}{n}) + +N(\bar{f}(\tau, \frac{1}{n})) - g(\tau)], \tag{13}$$

The deformation of topology is known as $\bar{f}(\tau, q)$ moves from $\bar{f}_0(\tau)$ to $\bar{f}(\tau)$ as moves from 0 to $\frac{1}{n}$. As wall $[D(\bar{f}(\tau, q)) - D(\bar{f}_0)]$ and $[D(\bar{f}(\tau)) + U(\bar{f}(\tau)) + N(\bar{f}(\tau))]$ are referred to as homotopic. The power series that we obtain after solving Eq. (11) is as follows

$$\bar{f}(\tau, q) = \sum_{m=0}^{\infty} \bar{f}_m(\tau) q^m, \tag{14}$$

The homotopy deformation equations provide the proper solutions for the coefficients $\bar{f}_m(\tau)$ in Eq. (14) [17]. Therefore, it is easy to obtain the approximate analytical solution of Eq. (10) as

$$\bar{f}(\tau) = \lim_{q \to \frac{1}{n}} \bar{f}(\tau, q) = \sum_{m=0}^{\infty} \bar{f}_m(\tau) \left(\frac{1}{n}\right)^m, \tag{15}$$

where

$$\bar{f}_m(\tau) = \frac{1}{m!} \frac{d^m \bar{f}(\tau, q)}{dq^m}\Big|_{q=0}, \tag{16}$$

Now, the Eq. (11) is derived m times with respect to q then set $q = 0$ with dividing the results by $m!$. The defining of the vector is $\vec{\bar{f}}_m(\tau) = \{\bar{f}_0(\tau), \bar{f}_1(\tau), \bar{f}(\tau), \dots, \bar{f}_m(\tau)\}$. The m^{th} order deformation equation can be represented as follow [14]

$$\bar{f}_m(\tau) = \delta_m\, \bar{f}_{m-1}(\tau)\ + hH(\tau) D^{-1}[R_m(\vec{\bar{f}}_{m-1}(\tau))], \tag{17}$$

where

$$R_m(\vec{\bar{f}}_{m-1}(\tau)) = \frac{1}{(m-1)!} \frac{d^{m-1}[D\left(\bar{f}(\tau,q)\right) + U\left(\bar{f}(\tau,q)\right) + N\left(\bar{f}(\tau,q) - g(\tau)\right)]}{dq^{m-1}}\Big|_{q=0}, \tag{18}$$

and

$$\delta_m = \begin{cases} 0 & m \leq 1 \\ n & otherwise \end{cases}, \tag{19}$$

It is important to note that the nonlinear Eq. (17) is given $\bar{f}_m(\tau)$ for $m \geq 1$ in the presence of linear boundary conditions for the original equation. The presence of the operator n increases the

probability of convergence or even allows much faster convergence than a standard HAM. It should be mentioned that standard HAM can be reached in the case of $n = 1$ in Eq. (11).

4. The Improvement of q- Homotopy Analysis Method

The main goal of this section is to improve the approximate analytical solutions resulting from q-HAM. This improvement includes two new techniques using the method imposed by two transforms: the Laplace transform and the EL-Zaki transform with the help of the convolution theorem can be summarize this improvement as

Hybridization q-Homotopy Analysis by Convolution Laplace Transform

Through this part, it can demonstrate the hybrid approach that combines the q-homotopy analysis method and the Laplace transform supported by convolution theory. By rewriting Eq. (10) with assume that the defining of the operator is $D = \frac{d^n}{d\tau^n}$ as the following

$$\frac{d^n \bar{f}(\tau)}{d\tau^n} + U(\bar{f}(\tau)) + N(\bar{f}(\tau)) - g(\tau) = 0, \tag{20}$$

Based on the Laplace transforms impact on both sides of Eq. (20), become

$$\mathcal{L}\left[\frac{d^n \bar{f}(\tau)}{d\tau^n} + U\big(\bar{f}(\tau)\big) + N\big(\bar{f}(\tau)\big) - g(\tau)\right] = 0, \tag{21}$$

The following results from the Laplace transform's properties for Eq. (21), yield

$$s^n \mathcal{L}\big[\bar{f}(\tau)\big] - \sum_{\omega=0}^{n-1} s^{n-\omega-1} \bar{f}^{(\omega)}(0) + \mathcal{L}\left[U\left(\bar{f}(\tau)\right) + N\left(\bar{f}(\tau)\right) - g(\tau)\right] = 0, \tag{22}$$

Rearranging Eq. (22) results in

$$\mathcal{L}\big[\bar{f}(\tau)\big] - \frac{1}{s^n}\sum_{\omega=0}^{n-1} s^{n-\omega-1} \bar{f}^{(\omega)}(0) + \frac{1}{s^n}\mathcal{L}\left[U\left(\bar{f}(\tau)\right) + N\left(\bar{f}(\tau)\right) - g(\tau)\right] = 0, \tag{23}$$

From the Laplace transform properties, we can put $\frac{1}{s^n} = \frac{\mathcal{L}[\tau^{n-1}]}{(n-1)!}$ in Eq. (23), the outcome is

$$\mathcal{L}\big[\bar{f}(\tau)\big] - \frac{1}{(n-1)!}\mathcal{L}[\tau^{n-1}]\sum_{\omega=0}^{n-1} s^{n-\omega-1} \bar{f}^{(\omega)}(0) + \frac{1}{(n-1)!}\mathcal{L}[\tau^{n-1}] \times \mathcal{L}\left[U\left(\bar{f}(\tau)\right) + N\left(\bar{f}(\tau)\right) - g(\tau)\right] = 0, \tag{24}$$

Now, the Eq. (24) can be rewrite as follows

$$\mathcal{L}\big[\bar{f}(\tau)\big] - \frac{1}{(n-1)!}\mathcal{L}[\tau^{n-1}]\sum_{\omega=0}^{n-1} s^{n-\omega-1} \bar{f}^{(\omega)}(0) + \mathcal{L}\left[\frac{\tau^{n-1}}{(n-1)!} * \left(U\left(\bar{f}(\tau)\right) + N\left(\bar{f}(\tau)\right) - g(\tau)\right)\right] = 0\,, \tag{25}$$

where the operation * is provided by

$$\mathcal{L}[\bar{f}(\tau) * \bar{g}(\tau)] = \mathcal{L}[\bar{f}(\tau) \times \bar{g}(\tau)],$$
$$\bar{f}(\tau) * \bar{g}(\tau) = \int_0^\tau \bar{f}(\tau - \xi)\bar{g}(\xi)d\xi,$$

By using the convolution theory concept of Eq. (25), the following outcome can be obtained

$$\mathcal{L}\left[\bar{f}(\tau)\right] - \frac{\mathcal{L}[\tau^{n-1}]}{(n-1)!}\sum_{\omega=0}^{n-1} s^{n-\omega-1}\bar{f}^{(\omega)}(0) + \mathcal{L}[\int_0^\tau \frac{(\tau-\xi)^{n-1}}{(n-1)!}(U(\bar{f}(\tau)) + N(\bar{f}(\tau))$$
$$-g\ (\tau)]|_{\tau=\xi}d\xi = 0, \tag{26}$$

Now, the nonlinear operator can be display as follow

$$B\left[\bar{f}(\tau,q)\right] = \mathcal{L}\left[\bar{f}(\tau)\right] - \frac{\mathcal{L}[\tau^{n-1}]}{(n-1)!}\sum_{\omega=0}^{n-1} s^{n-\omega-1}\bar{f}^{(\omega)}(0) + \mathcal{L}[\int_0^\tau \frac{(\tau-\xi)^{n-1}}{(n-1)!} \times (U\left(\bar{f}(\tau)\right) +$$
$$N(\bar{f}(\tau)) - g\ (\tau))\Big|_{\tau=\xi}d\xi\ ], \tag{27}$$

Hence, by taking Laplace transform for the first term of the Eq. (17), it results as

$$\mathcal{L}[\bar{f}_m(\tau) - \delta_m\ \bar{f}_{m-1}(\tau)] = hqH(\tau)[R_m(\vec{\bar{f}}_{m-1}(\tau))], \tag{28}$$

After taking the inverse of Laplace transform of the above equation, we can find the following

$$\bar{f}_m(\tau) = \delta_m\ \bar{f}_{m-1}(\tau) + hqH(\tau)\mathcal{L}^{-1}[R_m(\vec{\bar{f}}_{m-1}(\tau))], \tag{29}$$

where

$$R_m(\vec{\bar{f}}_{m-1}(\tau)) = \frac{1}{(m-1)!}\frac{d^{m-1}(B[\bar{f}(\tau,q)])]}{dq^{m-1}}\Big|_{q=0},$$

Hybridization q-Homotopy Analysis by Convolution EL- Zaki Transform

The Hybrid approach of the EL-Zaki transform, q-homotopy analysis method and convolution theory is presented to find the improvement solutions of q-HAM as following

Taking the EL- Zaki transform on both sides of Eq. (20), become

$$E\left[\frac{d^n\bar{f}}{d\tau^n} + U(\bar{f}) + N(\bar{f}) - g\ (\tau)\right] = 0, \tag{30}$$

Implementing in the EL-Zaki transform differentiation property for the equation, can explain the following results

$$\frac{E[\bar{f}(\tau)]}{J^n} - \sum_{\omega=0}^{n-1} J^{2-n+\omega}\bar{f}^{(\omega)}(0) + E\left[U\left(\bar{f}(\tau)\right) + N\left(\bar{f}(\tau)\right) - g(\tau)\right] = 0, \tag{31}$$

Rearranging Eq. (31) results in

$$E\left[\bar{f}(\tau)\right] - J^n \sum_{\omega=0}^{n-1} J^{2-n+\omega} \bar{f}^{(\omega)}(0) + J^n E\left[U\left(\bar{f}(\tau)\right) + N\left(\bar{f}(\tau)\right) - g(\tau)\right] = 0, \quad (32)$$

From The EL-Zaki transform properties, we can substitute $J^{n+2} = \frac{1}{n!} E[\tau^n]$ in Eq. (32), yield

$$E\left[\bar{f}(\tau)\right] - \frac{1}{n! J^2} E[\tau^n] \sum_{\omega=0}^{n-1} J^{2-n+\omega} \bar{f}^{(\omega)}(0) + \frac{1}{n! J^2} E[\tau^n] \times E[U(\bar{f}(\tau)) + N(\bar{f}(\tau)) - g(\tau)] = 0, \quad (33)$$

The Eq. (33) can be introduced by the following form

$$E\left[\bar{f}(\tau)\right] = \frac{1}{n! J^2} E[\tau^n] \sum_{\omega=0}^{n-1} J^{2-n+\omega} \bar{f}^{(\omega)}(0) + \frac{1}{J} E[\frac{1}{n!} \tau^n * (U\left(\bar{f}(\tau)\right) + N\left(\bar{f}(\tau)\right) - g(\tau))], \quad (34)$$

where the operation * is provided by
$E[\bar{f}(\tau) * \bar{g}(\tau)] = \frac{1}{J} E[\bar{f}(\tau) \times \bar{g}(\tau)]$,
$\bar{f}(\tau) * \bar{g}(\tau) = \int_0^\tau \bar{f}(\tau - \xi) \bar{g}(\xi) d\xi$,

Using the concept of convolution theory for the last term of Eq. (34), the following result can be obtained

$$E\left[\bar{f}(\tau)\right] - \frac{E[\tau^n]}{n! J^2} \sum_{\omega=0}^{n-1} J^{2-n+\omega} \bar{f}^{(\omega)}(0) + \frac{1}{J} E(\int_0^\tau \left(\frac{(\tau-\xi)^n}{n!} [U(\bar{f}(\tau)) + N(\bar{f}(\tau)) - g(\tau)]\Big|_{\tau=\xi}\right) d\xi) = 0, \quad (35)$$

Now, the nonlinear operator can be defined as follows

$$C\left[\bar{f}(\tau, q)\right] = E\left[\bar{f}(\tau)\right] - \frac{1}{n! J^2} E[\tau^n] \sum_{\omega=0}^{n-1} J^{2-n+\omega} \bar{f}^{(\omega)}(0) + \frac{1}{J} E[\frac{1}{n!} \tau^n * (U(\bar{f}(\tau)) + N(\bar{f}(\tau)) - g(\tau))], \quad (36)$$

Hence, by taking EL-Zaki transform for the first term of the Eq. (17), it results as

$$E[\bar{f}_m(\tau) - \delta_m \bar{f}_{m-1}(\tau)] = hqH(\tau)[R_m(\vec{\bar{f}}_{m-1}(\tau))], \quad (37)$$

After taking the inverse of EL-Zaki transform of the above equation, we can find the following

$$\bar{f}_m(\tau) = \delta_m \bar{f}_{m-1}(\tau) + hqH(\tau) E^{-1}[R_m(\vec{\bar{f}}_{m-1}(\tau))], \quad (38)$$

where,

$$R_m(\vec{\bar{f}}_{m-1}(\tau)) = \frac{1}{(m-1)!} \frac{d^{m-1}(C[\bar{f}(\tau,q)])}{dq^{m-1}}\Big|_{q=0},$$

Finally, Eq. (29) and Eq. (38) can be solved to find $\bar{f}_m(\tau), m = 1,2,3,\ldots$which is the approximate analytical solution, which can be expressed as a series containing the convergence parameters h and n. This solution is substituted into the Eq. (15), as the fraction factor $\left(\frac{1}{n}\right)^m$ present in Eq. (15) greatly increases the chances of convergence.

5. The Applications of Jeffery-Hamel Nano-Fluid Flow Problem by q-HAM, LTC-q-HAM and ETC-q-HAM

The implementation of q-HAM with its improvement to the nonlinear ordinary differential Eq. (7), to extract the approximate analytical solution. These applications can be explained below

$$\frac{d^3\bar{f}}{d\tau^3} + 2\varphi Re((1-w) + \frac{\hat{\rho}_s}{\hat{\rho}_f}w)(1-w)^{2.5}\bar{f}\frac{d\bar{f}}{d\tau} + (4-(1-w)^{1.25}Ha)\varphi^2\frac{d\bar{f}}{d\tau} = 0, \tag{39}$$

The assumption of the initial condition is

$$\bar{f}_0(\tau) = \Gamma_0 + \Gamma_1\tau + \Gamma_2\frac{\tau^2}{2!}, \tag{40}$$

where $\bar{f}(0) = \Gamma_0,\ \bar{f}'(0) = \Gamma_1, \bar{f}''(0) = \Gamma_2$.

The components of initial condition are readily found using Eq. (8) and Eq. (40) as follow

$$\bar{f}_0(\tau) = 1 + \Gamma_2\frac{\tau^2}{2!}, \tag{41}$$

According to Adomian polynomials of nonlinear term, a nonlinear operator is defined as follow

$$R_m(\vec{\bar{f}}_{m-1}(\tau)) = \frac{d^3\bar{f}_{m-1}}{d\tau^3} + 2\varphi Re((1-w) + \frac{\hat{\rho}_s}{\hat{\rho}_f}w)(1-w)^{2.5}\sum_{z=0}^{m-1}\sum_{s=0}^{z}\bar{f}_s\frac{d}{d\tau}\bar{f}_{m-1-z} +$$
$$(4-(1-w)^{1.25}Ha)\varphi^2\frac{d\bar{f}_{m-1}}{d\tau}, \quad m = 1,2,\ldots \tag{42}$$

Eq. (7) can now be solved to obtain

$$\bar{f}_m(\tau) = \delta_m\bar{f}_{m-1}(\tau) + hH(\tau)\int_0^\tau\int_0^\tau\int_0^\tau \frac{d^3\bar{f}_{m-1}}{d\tau^3} + 2\varphi Re((1-w) + \frac{\hat{\rho}_s}{\hat{\rho}_f}w)(1-w)^{2.5}$$
$$\sum_{z=0}^{m-1}\sum_{s=0}^{z}\bar{f}_s\frac{d}{d\tau}\bar{f}_{m-1-z} + (4-(1-w)^{1.25}Ha)\varphi^2\frac{d\bar{f}_{m-1}}{d\tau}, \tag{43}$$

The iterative approximate solutions with assume that $d = \frac{1}{\hat{\rho}_f}$ for the purpose of simplification as follows

$$\bar{f}_1(\tau) = (0.166666666\varphi^2\Gamma_2 h - 0.04166666665\varphi^2\Gamma_2(1-w)^{1.25}Hah + 0.08333333332$$
$$\varphi Re(1-w)^{2.5}\Gamma_2 h - 0.08333333332\varphi Re(1-w)^{2.5}\Gamma_2 wh + 0.08333333332\varphi Re(1-w)^{2.5}$$
$$\Gamma_2 w\hat{\rho}_s hd)\tau^4 + (0.008333333333\varphi Re(1-w)^{2.5}\Gamma_2^2 h - 0.00833333333\varphi Re(1-w)^{2.5}\Gamma_2^2 wh +$$
$$0.008333333333\varphi Re(1-w)^{2.5}\Gamma_2^2 w\hat{\rho}_s hd)\tau^6,$$
$$\bar{f}_2(\tau) = (-0.003240740741\varphi^2 Re^2\Gamma_2^3 w^3 h^2 + 0.003240740741\varphi^2 Re^2\Gamma_2^3 w^4 h^2 -$$

$0.001944444444\varphi^2 Re^2 \Gamma_2^3 w^5 h^2 + 0.0006481481482\varphi^2 Re^2 \Gamma_2^3 w^6 h^2 - 0.00009259259260$
$\varphi^2 Re^2 \Gamma_2^3 w^7 h^2 - 0.0006481481482\varphi^2 R_e^2 \Gamma_2^3 w h^2 + 0.001944444444\varphi^2 R_e^2 \Gamma_2^3 w^2 h^2 +$
$0.00009259259260\varphi^2 R_e^2 \Gamma_2^3 h^2 + 0.0001851851852\varphi^2 R_e^2 \Gamma_2^3 w^7 \hat{\rho}_s h^2 d -$
$0.001111111111\varphi^2 R_e^2 \Gamma_2^3 w^2 \hat{\rho}_s h^2 d + \cdots.$
$\vdots$

The remaining iterative components $\bar{f}_m(\tau), m = 3,4,5,6, \ldots$ can be obtained by similarity. The expression for the series solution by q-HAM can be expressed as follows

$$\bar{f}(\tau, n; h) \cong \bar{f}_m(\tau, n; h) = \sum_{i=0}^{m} u_i(\tau, n; h) \left(\frac{1}{n}\right)^i, \; n = 1,2, \ldots \tag{44}$$

The Application of LTC-q-HAM to find the approximate analytical solution by taking the Laplace transform to both sides of Eq. (7), become

$$\mathcal{L}[\frac{d^3 \bar{f}}{d\tau^3}] + 2\varphi Re((1-w) + \frac{\hat{\rho}_s}{\hat{\rho}_f} w)(1-w)^{2.5} \mathcal{L}[\bar{f} \frac{d\bar{f}}{d\tau}] + (4 - (1-w)^{1.25} Ha)\varphi^2 \mathcal{L}[\frac{d\bar{f}}{d\tau}] = 0, \tag{45}$$

By implementing the initial condition from Eq. (45), and the differentiation property of the Laplace transform, yield

$$\mathcal{L}[\bar{f}] - (\frac{s^2 + \Gamma_2}{s^3}) + \frac{1}{s^3} \mathcal{L}[2\varphi Re((1-w) + \frac{\hat{\rho}_s}{\hat{\rho}_f} w)(1-w)^{2.5} \bar{f} \frac{d\bar{f}}{d\tau} + (4 - (1-w)^{1.25} Ha)\varphi^2 \frac{d\bar{f}}{d\tau}] = 0, \tag{46}$$

From the Laplace transform's properties substituting $\frac{1}{s^3} = \frac{1}{2!} \mathcal{L}[\tau^2]$ the following results

$$\mathcal{L}[\bar{f}] - (\frac{s^2 + \Gamma_2}{s^3}) + \frac{1}{2!} \mathcal{L}[\tau^2] \times \mathcal{L}[2\varphi Re((1-w) + \frac{\hat{\rho}_s}{\hat{\rho}_f} w)(1-w)^{2.5} \bar{f} \frac{d\bar{f}}{d\tau} +$$
$$(4 - (1-w)^{1.25} Ha)\varphi^2 \frac{d\bar{f}}{d\tau}] = 0, \tag{47}$$

By utilizing the convolution theory concept on the last term of Eq. (47), the following outcome can be obtained

$$\mathcal{L}[\bar{f}] - (\frac{s^2 + \Gamma_2}{s^3}) + \mathcal{L}[\frac{1}{2!} \tau^2 * (2\varphi Re((1-w) + \frac{\hat{\rho}_s}{\hat{\rho}_f} w)(1-w)^{2.5} \bar{f} \frac{d\bar{f}}{d\tau}) + (4 - (1-w)^{1.25} Ha)$$
$$\varphi^2 \frac{d\bar{f}}{d\tau})] = 0, \tag{48}$$

The following results from taking the inverse Laplace transform of both sides of Eq. (48) and from q-HAM we obtain

$$\bar{f}_m(\tau) = \delta_m \bar{f}_{m-1}(\tau) + h\mathcal{L}^{-1}(\mathcal{L}[\bar{f}_{m-1}] - \left(\frac{s^2 + \Gamma_2}{s^3}\right)\left(1 - \frac{1}{n}\delta_m\right)) + \frac{h}{2!} \int_0^\tau ((\tau - \xi)^2 [2\varphi Re((1-w) +$$
$$\frac{\hat{\rho}_s}{\hat{\rho}_f} w)(1-w)^{2.5} \sum_{z=0}^{m-1} \sum_{s=0}^{z} \bar{f}_s \frac{d}{d\tau} \bar{f}_{m-1-z} + (4 - (1-w)^{1.25} Ha)\, \varphi^2 \frac{d}{d\xi} \bar{f}_{m-1}]\Big|_{\tau=\xi}) \, d\xi \tag{49}$$

$\bar{f}_1(\tau) = (0.166666666\varphi^2\Gamma_2 h - 0.04166666665\ \varphi^2\Gamma_2(1-w)^{1.25}Hah + 0.08333333330$
$\varphi Re(1-w)^{2.5}\Gamma_2 h - 0.08333333330\varphi\ R_e(1-w)^{2.5}\Gamma_2 wh + 0.08333333330\varphi R_e(1-w)^{2.5}$
$\Gamma_2 w\hat{\rho}_s hd)\tau^4 + (0.008333333350\varphi R_e(1-w)^{2.5}\Gamma_2^2 h - 0.00833333350\varphi R_e(1-w)^{2.5}\Gamma_2^2 wh +$
$0.008333333350\varphi Re(1-w)^{2.5}\Gamma_2^2 w\hat{\rho}_s hd)\tau^6$
$\bar{f}_2(\tau) = (-0.003240740750\varphi^2 R_e^2\Gamma_2^3 w^3 h^2 + 0.003240740750\varphi^2 R_e^2\Gamma_2^3 w^4 h^2 - 0.001944444500$
$\varphi^2 R_e^2\Gamma_2^3 w^5 h^2 + 0.0006481481550\varphi^2 R_e^2\Gamma_2^3 w^6 h^2 - 0.00009259259350\varphi^2 R_e^2\Gamma_2^3 w^7 h^2 -$
$0.0006481481550\varphi^2 R_e^2\Gamma_2^3 wh^2 + 0.001944444500\varphi^2 R_e^2\Gamma_2^3 w^2 h^2 + 0.00009259259350$
$\varphi^2 R_e^2\Gamma_2^3 h^2 + 0.0001851851850\varphi^2 R_e^2\Gamma_2^3 w^7\hat{\rho}_s h^2 d - 0.001111111120\varphi^2 R_e^2\Gamma_2^3 w^2\hat{\rho}_s h^2 d + \cdots.$
$\vdots$

The application of ZTC-q-HAM to find the approximate analytical solution by taking the EL-Zaki transform to both sides of Eq. (7), output

$$E[\frac{d^3\bar{f}}{d\tau^3}] + 2\varphi Re((1-w) + \frac{\hat{\rho}_s}{\hat{\rho}_f}w)(1-w)^{2.5}E[\bar{f}\frac{d\bar{f}}{d\tau}] + (4-(1-w)^{1.25}Ha)\ \varphi^2 E[\frac{d\bar{f}}{d\tau}] = 0, \quad (50)$$

by the initial condition from Eq. (50), and the differentiation properties of the EL-Zaki transform, yield

$$E[\bar{f}] - (J^2 + J^4\Gamma_2) + J^3 E[2\varphi Re((1-w) + \frac{\hat{\rho}_s}{\hat{\rho}_f}w)(1-w)^{2.5}\bar{f}\frac{d\bar{f}}{d\tau} + (4-(1-w)^{1.25}Ha)$$
$$\varphi^2\frac{d\bar{f}}{d\tau}] = 0, \quad (51)$$

The following results from the EL-Zaki transform properties

$$E\big[\bar{f}\big] - (J^2 + J^4\Gamma_2) + E[\tau] \times E[2\varphi Re((1-w) + \frac{\hat{\rho}_s}{\hat{\rho}_f}w)(1-w)^{2.5}\bar{f}\frac{d\bar{f}}{d\tau} + (4-(1-w)^{1.25}Ha)$$
$$\varphi^2\frac{d\bar{f}}{d\tau}] = 0, \quad (52)$$

By using the convolution theory concept on the last term of Eq. (52), the following outcome can be obtained

$$E[\bar{f}] - (J^2 + J^4\Gamma_2) + JE[(\tau) * (2\varphi Re((1-w) + \frac{\hat{\rho}_s}{\hat{\rho}_f}w)(1-w)^{2.5}\bar{f}\frac{d\bar{f}}{d\tau} + (4-(1-w)^{1.25}Ha)$$
$$\varphi^2\frac{d\bar{f}}{d\tau})] = 0\ , \quad (53)$$

The following results from taking the inverse EL-Zaki transform of both sides of Eq. (53) and from q-HAM, become

$$R_m(\vec{\bar{f}}_{m-1}(\tau)) = E[\bar{f}_{m-1}] - (J^2 + J^4\Gamma_2)(1-\frac{1}{n}\delta_m) + JE[(\tau) * (2\varphi Re((1-w) + \frac{\hat{\rho}_s}{\hat{\rho}_f}w)(1-$$
$$w)^{2.5}\sum_{z=0}^{m-1}\sum_{s=0}^{z}\bar{f}_s\frac{d\bar{f}_{m-1-z}}{d\tau} + (4-(1-w)^{1.25}Ha)\varphi^2\frac{d}{d\tau}\bar{f}_{m-1}, \quad (54)$$

and

$$\bar{f}_m(\tau) = \delta_m\bar{f}_{m-1}(\tau) + hE^{-1}(E[\bar{f}_{m-1}] - (J^2 + J^4\Gamma_2)(1-\frac{1}{n}\delta_m) + JE[(\tau) * 2\varphi Re((1-w) +$$

$$\frac{\hat{\rho}_s}{\hat{\rho}_f}w)(1-w)^{2.5} + \sum_{z=0}^{m-1}\sum_{s=0}^{z}\bar{f}_s\frac{d\bar{f}_{m-1-z}}{d\tau}(4-(1-w)^{1.25}Ha)), \quad (55)$$

The following is a description of Eq. (55)

$$\bar{f}_m(\tau) = \delta_m\bar{f}_{m-1}(\tau) + hE^{-1}(E\left[\bar{f}_{m-1}\right] - (J^2 + J^4\Gamma_2)(1-\frac{1}{n}\delta_m)) + hE^{-1}$$
$$[JE(\int_0^\tau((\tau-\xi)\times 2\varphi Re((1-w)+\frac{\hat{\rho}_s}{\hat{\rho}_f}w)(1-w)^{2.5}\sum_{z=0}^{m-1}\sum_{s=0}^{z}\bar{f}_s\frac{d}{d\tau}\bar{f}_{m-1-z} +$$
$$(4-(1-w)^{1.25}Ha)\,\varphi^2\frac{d}{d\xi}\bar{f}_{m-1}]\Big|_{\tau=\xi})\,d\xi, \quad (56)$$

The iterations analytical of the solution can be defined by the following

$$\bar{f}_1(\tau) = (0.1666666667\varphi^2\Gamma_2 h - 0.04166666668\varphi^2\Gamma_2(1-w)^{1.25}Hah + 0.08333333337$$
$$\varphi Re(1-w)^{2.5}\Gamma_{12}h - 0.08333333337\varphi R_e(1-w)^{2.5}\Gamma_2 wh + 0.08333333337\varphi R_e(1-w)^{2.5}$$
$$\Gamma_2 w\hat{\rho}_s hd)\tau^4 + (0.008333333335\varphi R_e(1-w)^{2.5}\Gamma_2^2 h - 0.008333333335\varphi R_e(1-w)^{2.5}\Gamma_2^2 wh +$$
$$0.008333333335\varphi Re(1-w)^{2.5}\Gamma_2^2 w\hat{\rho}_s h\,d)\tau^6,$$
$$\bar{f}_2(\tau) = (-0.003240740744\varphi^2 R_e^2\Gamma_2^3 w^3h^2 + 0.003240740744\varphi^2 R_e^2\Gamma_2^3 w^4h^2 - 0.001944444447$$
$$\varphi^2 R_e^2\Gamma_2^3 w^5h^2 + 0.0006481481484\varphi^2 R_e^2\Gamma_2^3 w^6h^2 - 0.00009259259268\varphi^2 R_e^2\Gamma_2^3 w^7h^2 -$$
$$0.0006481481484\varphi^2 R_e^2\Gamma_2^3 wh^2 + 0.001944444446\varphi^2 R_e^2\Gamma_2^3 w^2h^2 + 0.00009259259268$$
$$\varphi^2 R_e^2\Gamma_2^3 h^2 + 0.0001851851854\varphi^2 R_e^2\Gamma_2^3 w^7\hat{\rho}_s h^2 d - 0.001111111112\varphi^2 R_e^2\Gamma_2^3 w^2\hat{\rho}_s h^2 d + \cdots.$$
$$\vdots$$

6. Findings and Discussions

The influence of various flow parameters (Hartmann, nanofluid volume fraction, and Reynold numbers) on the velocity profile $\bar{f}(\tau)$ is studied for magneto-hydrodynamic Jeffrey-Hamel flow with nanoparticles. Table 2 to Table 7 indicate the convergence of the values of Γ_2 which can see these values are constant in fourth-order. Between the numerical solution obtained by the bvp4c, method and the modified q-HAM method. Next the tables and the figures that show the effect the physical parameters of Re, Ha, and w on the velocity as follow will be examined:

Table 2
The convergence of the value Γ_2 for material Al_2O_3 when $n = 1.5, h = -1.5, Ha = 0, Re = 10, \varphi = 3^{\circ}, w = 0.01$

Approximates	q-HAM	ZT-q-HAM	ZTC-q-HAM	LTC-q-HAM	bvp4c
1 order	-2.14978889	-2.14978889	-2.14978550	-2.14978550	-2.14698216
2 order	-2.14700857	-2.14700856	-2.14700529	-2.14700529	-2.14698216
3 order	-2.14695797	-2.14695797	-2.14695470	-2.14695470	-2.14698216
4 order	-2.14696040	-2.14696039	-2.14695715	-2.14695713	-2.14696039
5 order	-2.14696040	-2.14696039	-2.14695715	-2.14695713	-2.14696039
6 order	-2.14696040	-2.14696039	-2.14695715	-2.14695713	-2.14696039

Table 3
The convergence of the value Γ_2 for material TiO_2 when $n = 1.5, h = -1.5, Ha = 0, Re = 10, \varphi = 3^{\circ}, w = 0.01$

Approximates	q-HAM	ZT-q-HAM	ZTC-q-HAM	LTC-q-HAM	bvp4c
1 order	-2.15021364	-2.15021364	-2.15021331	-2.15021330	-2.14739143
2 order	-2.14741821	-2.14741821	-2.14741788	-2.14741788	-2.14739143
3 order	-2.14736716	-2.14736716	-2.14736684	-2.14736683	-2.14739143
4 order	-2.14736962	-2.14736961	-2.14736930	-2.14736929	-2.14736961
5 order	-2.14736962	-2.14736961	-2.14736930	-2.14736929	-2.14736961
6 order	-2.14736962	-2.14736961	-2.14736930	-2.14736929	-2.14736961

Table 4
The convergence of the value Γ_2 for material Cu when $n = 1.5, h = -1.5, Ha = 0, Re = 10, \varphi = 3^{\circ}, w = 0.01$

Approximates	q-HAM	ZT-q-HAM	ZTC-q-HAM	LTC-q-HAM	bvp4c
1 order	-2.15733521	-2.15733521	-2.15733485	-2.15733485	-2.15424749
2 order	-2.15428092	-2.15428092	-2.15428057	-2.15428057	-2.15424749
3 order	-2.15422184	-2.15422184	-2.15422149	-2.15422149	-2.15424749
4 order	-2.15422479	-2.15422478	-2.15422444	-2.15422444	-2.15422477
5 order	-2.15422479	-2.15422478	-2.15422444	-2.15422444	-2.15422477
6 order	-2.15422479	-2.15422478	-2.15422444	-2.15422444	-2.15422477

Table 5
The convergence of the value Γ_2 for material Al_2O_3 when $n = 1.5, h = -1.5, Ha = 600, Re = 30, \varphi = 5^{\circ}, w = 0.02$

Approximates	q-HAM	ZT-q-HAM	ZTC-q-HAM	LTC-q-HAM	bvp4c
1 order	-1.96940561	-1.96940561	-1.96940530	-1.96940530	-1.97126566
2 order	-1.97099526	-1.97099526	-1.97099492	-1.97099493	-1.97126566
3 order	-1.97104813	-1.97104814	-1.97104780	-1.97104781	-1.97104783
4 order	-1.97104784	-1.97104784	-1.97104751	-1.97104752	-1.97104783
5 order	-1.97104780	-1.97104780	-1.97104747	-1.97104747	-1.97104779
6 order	-1.97104780	-1.97104780	-1.97104747	-1.97104747	-1.97104779

Table 6
The convergence of the value Γ_2 for material TiO_2 when $n = 1.5, h = -1.5, Ha = 600, Re = 30, \varphi = 5^{\circ}, w = 0.02$

Approximates	q-HAM	ZT-q-HAM	ZTC-q-HAM	LT-q-HAM	bvp4c
1 order	-1.97275132	-1.97275132	-1.97275100	-1.97275100	-1.9748169
2 order	-1.97454546	-1.97454546	-1.97454513	-1.97454513	-1.9748169
3 order	-1.97459954	-1.97459954	-1.97459921	-1.97459921	-1.9745989
4 order	-1.97459901	-1.97459901	-1.97459867	-1.97459867	-1.9745989
5 order	-1.97459896	-1.97459896	-1.97459863	-1.97459862	-1.9745989
6 order	-1.97459896	-1.97459896	-1.97459863	-1.97459862	-1.9745989

Table 7
The convergence of the value Γ_2 for material Cu when $n = 1.5, h = -1.5, Ha = 600, Re = 30, \varphi = 5^{\circ}, w = 0.02$

Approximates	q-HAM	ZT-q-HAM	ZTC-q-HAM	LTC-q-HAM	bvp4c
1 order	-2.02985299	-2.02985299	-2.02985269	-2.02985271	-2.03511598
2 order	-2.03492345	-2.03492345	-2.03492314	-2.03492316	-2.03511598
3 order	-2.03490711	-2.03490712	-2.03490681	-2.03490683	-2.03489830
4 order	-2.03489832	-2.03489832	-2.03489801	-2.03489803	-2.03489830
5 order	-2.03489827	-2.03489826	-2.03489796	-2.03489798	-2.03489827
6 order	-2.03489827	-2.03489826	-2.03489796	-2.03489798	-2.03489827

The solutions series of q-HAM, ZT-q-HAM, LTC-q-HAM and ZTC-q-HAM represented tabular in Table 8 to Table 12 can be compared with numerical solutions which extracted from bvp4c method, other method such as HAM, SHAM, HPM, ADM and RVIM the methods of reference [7,9,18-20]. From this comparison can find that the q-HAM method using transformations with torsion theory is closer to the numerical solution than the q-HAM method and other methods that were compared and referred to

Table 8
The profile $\bar{f}(\tau)$ for Cu when $n = 1.6, h = -1.5, Ha = 0, Re = 50, \varphi = 5^{\circ}, w = 0$

τ	bvp4c	HPM [18]	Motsa *et al.,* [9]	ZTC-q-HAM	LTC-q-HAM
0.00	1.0000000000	1.000000	1.000000	1.000000000	1.0000000000
0.25	0.8942690802	0.894960	0.894242	0.8942691500	0.8942691498
0.50	0.6270207185	0.627220	0.626948	0.6270209668	0.6270209673
0.75	0.3020638643	0.302001	0.301991	0.3020643594	0.3020643606
1.00	0.0000000000	0.000000	0.000000	0.000000000	0.0000000000

Table 9
The profile $\bar{f}(\tau)$ for Cu when $n = 1.6, h = -1.5, Ha = 0, Re = 50, \varphi = 5^{\circ}, w = 0$

τ	bvp4c	q-HAM	ZT-q-HAM	Ganji *et al.,* [7]	SHPM [18]
0.00	1.0000000000	1.0000000000	1.0000000000	1.000000	1.000000
0.25	0.8942690802	.8942691505	0.8942691494	0.894243	0.894242
0.50	0.6270207185	0.6270209660	0.6270209669	0.626953	0.626948
0.75	0.3020638643	0.3020643597	0.3020643587	0.301998	0.301990
1.00	0.0000000000	0.0000000000	0.0000000000	0.000000	0.000000

Table 10
The profile of $\bar{f}(\tau)$ for Cu when $n = 1.5, h = -1.5, Ha = 750, Re = 10, \varphi = -5^{\circ}, w = 0.05$

τ	q-HAM	ZT-q-HAM	ZTC-q-HAM	LTC-q-HAM	Collocation method [19]
0.00	1.000000000	1.000000000	1.0000000000	1.0000000000	1.000000000
0.10	0.9942694612	0.9942694613	0.9942694612	0.9942694612	0.994278317
0.20	0.9766480441	0.9766480442	0.9766480439	0.9766480439	0.976670165
0.30	0.9458186628	0.9458186630	0.9458186622	0.9458186622	0.945855446
0.40	0.8994935422	0.8994935425	0.8994935413	0.8994935413	0.899546175
0.50	0.8342745286	0.8342745292	0.8342745274	0.8342745274	0.834341990
0.60	0.7454579170	0.7454579178	0.7454579154	0.7454579154	0.745536091
0.70	0.6267890703	0.6267890713	0.6267890684	0.6267890683	0.626869073
0.80	0.4701816709	0.4701816723	0.4701816693	0.4701816691	0.470248162
0.90	0.2654336979	0.2654336997	0.2654336969	0.2654336970	0.265469361
1.00	0.0000000000	0.0000000000	0.0000000000	0.0000000000	0.000000000

Table 11
The profile $\bar{f}(\tau)$ for Cu when $n = 1.5, h = -1.5, Ha = 0, Re = 25, \varphi = 5^{\circ}, w = 0$

τ	q-HAM	ZT-q-HAM	ZTC-q-HAM	LTC-q-HAM	bvp4c
0.00	1.0000000000	1.0000000000	1.0000000000	1.0000000000	1.0000000000
0.10	0.9866705485	0.9866705482	0.9866705481	0.9866705482	0.9866705482
0.20	0.9472577634	0.9472577637	0.9472577630	0.9472577637	0.9472577634
0.30	0.8834189782	0.8834189775	0.8834189773	0.8834189786	0.8834189781
0.40	0.7976973677	0.7976973687	0.7976973682	0.7976973679	0.7976973689
0.50	0.6932327502	0.6932327506	0.6932327507	0.6932327505	0.6932327508
0.60	0.5734244590	0.5734244593	.05734244594	0.5734244595	0.5734244599
0.70	0.4415925507	0.4415925518	0.4415925513	0.4415925528	0.4415925527
0.80	0.3006744137	0.3006744139	0.3006744136	0.3006744155	0.3006744156
0.90	0.1529785214	0.1529785219	0.1529785219	0.152978520	0.1529785231
1.00	0.0000000000	0.0000000000	0.0000000000	0.0000000000	0.0000000000

Table 12
The profile $\bar{f}(\tau)$ for Cu when $n = 1.5, h = -1.5, Ha = 0, Re = 25, \varphi = 5^{\circ}, w = 0$

τ	ADM [20]	RVIM [20]	bvp4c
0.00	1.000000	1.000000000	1.0000000000
0.10	0.986637	0.986669331	0.9866705482
0.20	0.947127	0.947253132	0.9472577634
0.30	0.883146	0.883409402	0.8834189781
0.40	0.797259	0.797682307	0.7976973689
0.50	0.692638	0.693212823	0.6932327508
0.60	0.572716	0.573401458	0.5734244599
0.70	0.44085	0.441569310	0.4415925527
0.80	0.300013	0.3006545894	0.3006744156
0.90	0.152552	0.152966340	0.1529785231
1.00	0.000000	0.000000000	0.0000000000

As wall as, in Table 13 to Table 17 can be seen that an improvement in the solutions obtained by the standard method (q-HAM) with the improved solutions using transformations and convolution theory by comparing them with the solutions obtained from the numerical method (bvp4c). Through these tables, the absolute error was extracted and it was found ZT-q HAM, LTC-q-HAM and ZTC-q-HAM, be more accurate than q-HAM. The outcome can be represented graphical as follow

Table 13
The comparison of $\bar{f}(\tau)$ between q-HAM, Zq-HAM, ZTC-q-HAM and LTC-q-HAM for Cu when $n = 1.5, h = -1.5, Ha = 600, Re = 30, \varphi = 5^{\circ}, w = 0.02$

τ	q-HAM	ZT-q-HAM	ZTC-q-HAM	LTC-q-HAM	bvp4c
0.00	1.0000000000000	1.0000000000000	1.0000000000000	1.0000000000000	1.000000000000000
0.10	.09898368266122	0.9898368266222	0.9898368268609	0.9898368268609	0.989836826859735
0.20	0.9594781365329	0.9594781365728	0.9594781375245	0.9594781375245	.0959478137520687
0.30	.09092794408976	0.9092794409869	0.9092794431179	0.9092794431179	.0909279443109950
0.40	.08397124787543	0.8397124789122	0.8397124826841	0.8397124826831	0.839712482668596
0.50	.07511914970770	0.7511914973223	0.7511915031910	0.7511915031910	0.751191503169716
0.60	0.6438406610775	0.6438406614291	0.6438406699767	0.6438406699777	0.643840669944824
0.70	0.5172038064203	0.5172038068976	0.5172038199121	.05172038199121	0.517203819867471
0.80	0.3698855760532	0.3698855766771	0.3698856011103	.03698856011103	.0369885601047807
0.90	0.1990915906856	0.1990915914799	0.1990916372593	0.1990916372603	0.199091637163935
1.00	0.0000000000000	0.0000000000000	0.0000000000000	0.0000000000000	0.000000000000000

Table 14
The comparison of the errors of $\bar{f}(\tau)$ between q-HAM, ZT-q-HAM, ZTC-q-HAM and LTC-q- HAM for Cu when $n = 1.5, h = -1.5, Ha = 600, Re = 30, \varphi = 5^{\circ}, w = 0.02$

τ	Absolute error q-HAM	Absolute error ZT-q-HAM	Absolute error ZTC-q-HAM	Absolute error LTC-q-HAM
0.00	0.000000000	0.000000000	0.000000000	0.000000000
0.10	2.47×10^{-10}	2.37×10^{-10}	1.16×10^{-12}	1.16×10^{-12}
0.20	9.87×10^{-10}	9.47×10^{-10}	3.81×10^{-12}	3.81×10^{-12}
0.30	2.21×10^{-9}	2.12×10^{-9}	7.94×10^{-12}	7.94×10^{-12}
0.40	3.91×10^{-9}	3.75×10^{-9}	1.55×10^{-11}	1.45×10^{-11}
0.50	6.09×10^{-9}	5.84×10^{-9}	2.12×10^{-11}	2.12×10^{-11}
0.60	8.86×10^{-9}	8.51×10^{-9}	3.18×10^{-11}	3.28×10^{-11}
0.70	1.34×10^{-8}	1.29×10^{-8}	4.46×10^{-11}	4.46×10^{-11}
0.80	2.49×10^{-8}	2.43×10^{-8}	6.24×10^{-11}	6.24×10^{-11}
0.90	4.64×10^{-8}	4.56×10^{-8}	9.53×10^{-11}	9.63×10^{-11}
1.00	0.000000000	0.000000000	0.000000000	0.000000000

Table 15
The comparison of $\bar{f}(\tau)$ between q-HAM, ZT-q-HAM, ZTC-q-HAM and LTC-q-HAM for Al_2O_3 when $n = 1.5, h = -1.5, Ha = 0, Re = 10, \varphi = 3^{\circ}, w = 0.01$

τ	q-HAM	ZT-q-HAM	ZTC-q-HAM	LTC-q-HAM	bvp4c
0.00	1.0000000000000	1.0000000000000	1.000000000000	1.0000000000000	1.0000000000000
0.10	0.9892746754293	0.9892746754293	0.9892746755100	0.9892746755100	0.9892746755094
0.20	0.9572113071006	0.9572113071006	0.9572113074190	0.9572113074190	0.9572113074203
0.30	0.9041393496163	0.9041393496163	0.9041393503310	0.9041393503310	0.9041393503325
0.40	0.8305804759233	0.8305804759233	0.8305804771860	0.8305804771850	0.8305804771885
0.50	0.7372089741221	0.7372089741223	0.7372089760800	0.7372089760780	0.7372089760819
0.60	0.6247991280628	0.6247991280633	0.6247991308320	0.6247991308270	0.6247991308340
0.70	0.4941619169730	0.4941619169743	0.4941619205260	0.4941619205150	0.4941619205253
0.80	0.3460734065680	0.3460734065711	0.3460734103460	0.3460734103230	0.3460734103420
0.90	0.1811968726728	0.1811968726793	0.1811968750510	0.1811968750100	0.1811968750453
1.00	0.0000000000000	0.0000000000000	0.0000000000000	0.0000000000000	0.0000000000000

Table 16
The comparison of the errors of $\bar{f}(\tau)$ between q-HAM, ZT-q-HAM, ZTC-q-HAM and LTC-q-HAM for Al_2O_3 when $n = 1.5, h = -1.5, Ha = 0, Re = 10, \varphi = 3^{\circ}, w = 0.01$

τ	Absolute error q-HAM	Absolute error ZT-q-HAM	Absolute error ZTC-q-HAM	Absolute error LTC-q-HAM
0.00	0.000000000	0.00000000	0.00000000	0.00000000
0.10	8.01×10^{-11}	8.01×10^{-11}	5.69×10^{-13}	5.69×10^{-13}
0.20	3.19×10^{-10}	3.19×10^{-10}	1.34×10^{-12}	1.34×10^{-12}
0.30	7.16×10^{-10}	7.16×10^{-10}	1.56×10^{-12}	1.56×10^{-12}
0.40	1.26×10^{-9}	1.26×10^{-9}	2.50×10^{-12}	3.50×10^{-12}
0.50	1.95×10^{-9}	1.95×10^{-9}	1.99×10^{-12}	3.99×10^{-12}
0.60	2.77×10^{-9}	2.77×10^{-9}	2.03×10^{-12}	7.03×10^{-12}
0.70	3.55×10^{-9}	3.55×10^{-9}	6.33×10^{-13}	1.03×10^{-11}
0.80	3.77×10^{-9}	3.77×10^{-9}	4.00×10^{-12}	1.89×10^{-11}
0.90	2.37×10^{-9}	2.36×10^{-9}	5.65×10^{-12}	3.53×10^{-11}
1.00	0.00000000	0.000000000	0.000000000	0.000000000

Table 17
Comparison of computed errors of $\bar{f}(\tau)$ between q-HAM, ZTC-q-HAM and LTC-q-HAM when $n = 1.5, h = -1.5, Ha = 0, Re = 10, \varphi = 3^{\circ}, w = 0.01$, $Al_2O_3 = 3970$

error	q-HAM	Zq-HAM	ZTC-q-HAM	LTC-q-HAM
L_1	7.52×10^{-11}	7.52×10^{-11}	1.52×10^{-11}	1.32×10^{-13}
L_2	8.67×10^{-6}	8.67×10^{-6}	3.90×10^{-6}	3.64×10^{-7}
L_∞	1.51×10^{-5}	1.51×10^{-5}	9.41×10^{-6}	6.28×10^{-7}

Material Al_2O_3

Figure 3 proves the effect Hartmann number for divergent and convergent channel on the velocity profiles. The findings indicate that a rise in Hartmann number causes the velocity profiles of divergent and convergent channels to increase. Therefore, increasing the Hartmann number shows that there hasn't been any backflow in either of the channels. Figure 4 illustrates that when channel is divergent, the fluid velocity decreases with Reynolds numbers, but when channel is convergent, the fluid velocity increases with Reynolds numbers. Most notably, as Figure 5 illustrates, when the nanofluid volume fraction rises, the fluid velocity increases in the case of convergent channels but falls in the case of divergent channels.

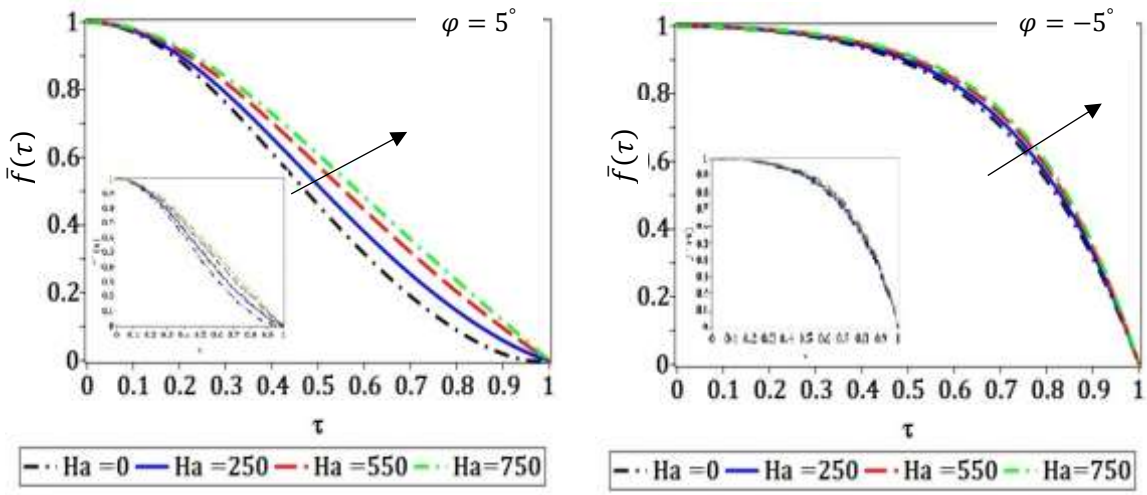

Fig. 3. Ha changed to Re $= 100, w = 0.05$ for Al_2O_3

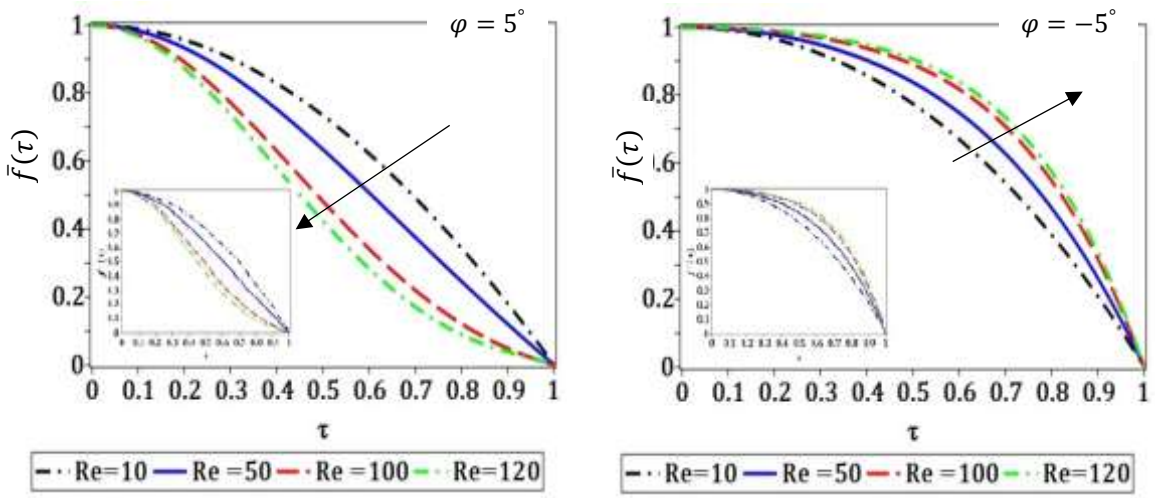

Fig. 4. Re changed to Ha $= 50, w = 0.05$ for Al_2O_3

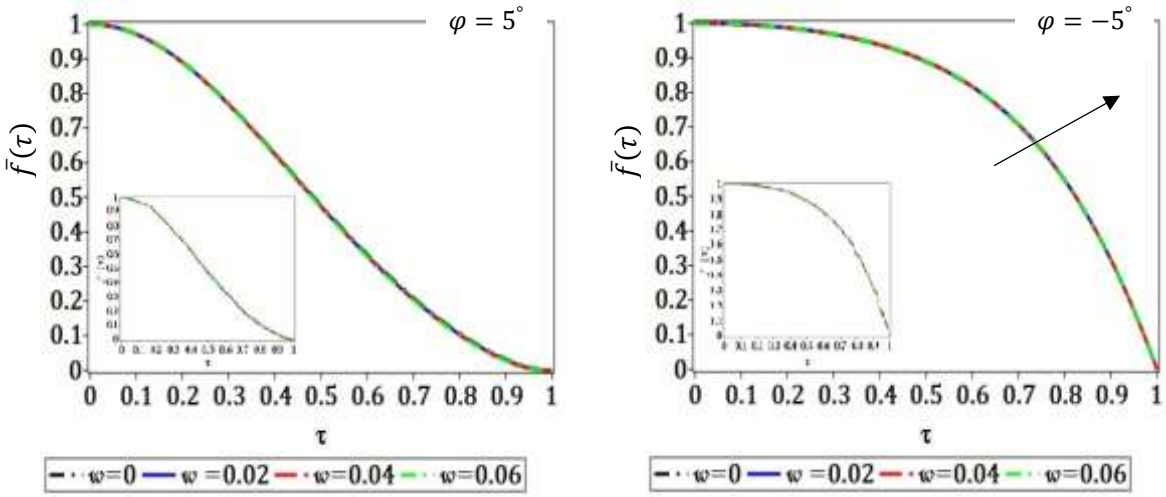

Fig. 5. w changed to Re $= 100$, Ha = 50 for Al_2O_3

Material TiO_2

In divergent and convergent channels, the velocity profiles with increasing Hartmann numbers are displayed in Figure 6. As a result, the velocity profiles become smaller. Accordingly, no backflow occurs in both channels as the Hartmann number increases. As the Reynolds number increases in both divergent and convergent channels, Figure 7 illustrates how the fluid velocity drops. According to Figure 8, when the nanofluid volume fraction increases, the fluid velocity falls in the case of divergent channel but increases with the nanofluid volume fraction in the case of convergent channel.

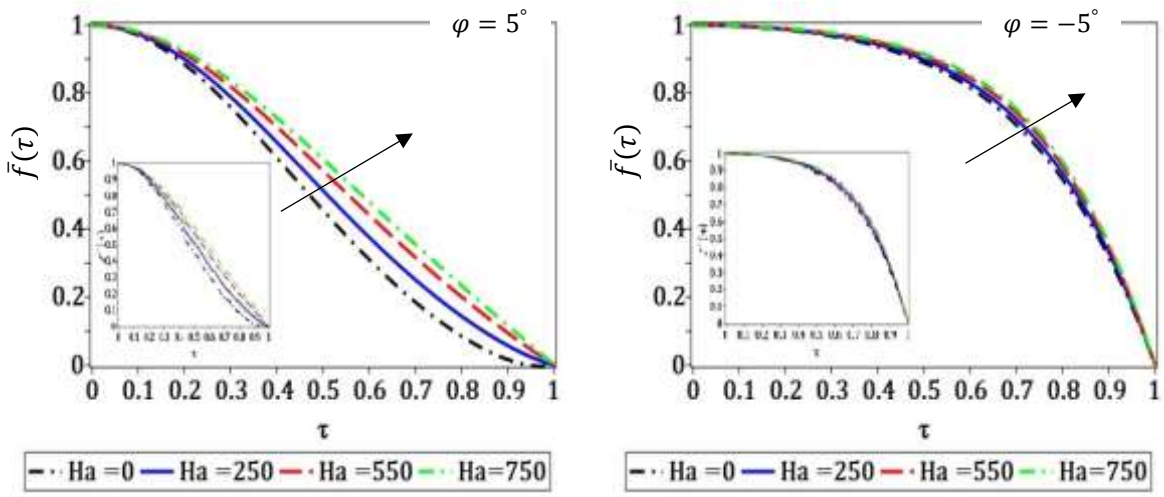

Fig. 6. Ha changed to Re $= 100, w = 0.05$ for TiO_2

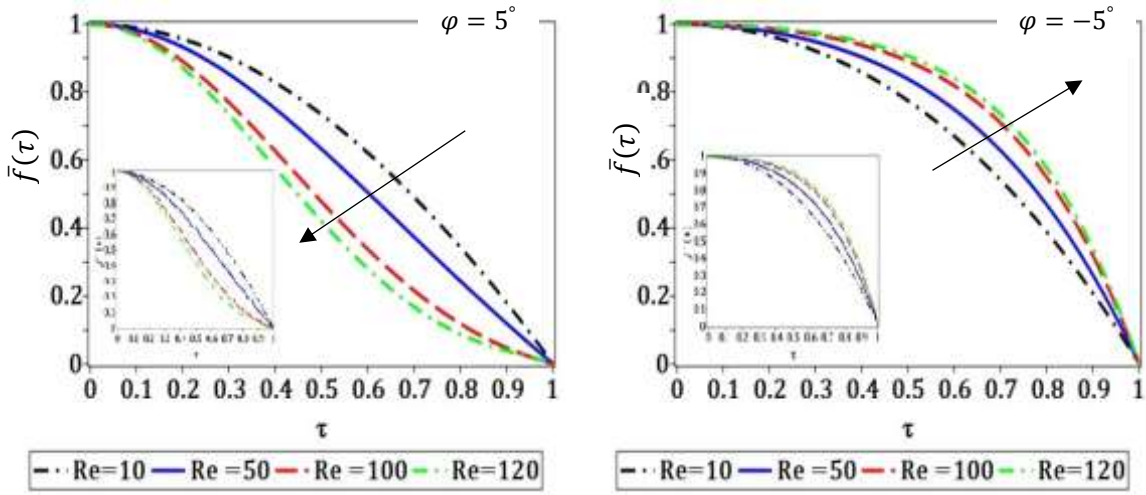

Fig. 7. Re changed to Ha $= 50, w = 0.05$ for TiO_2

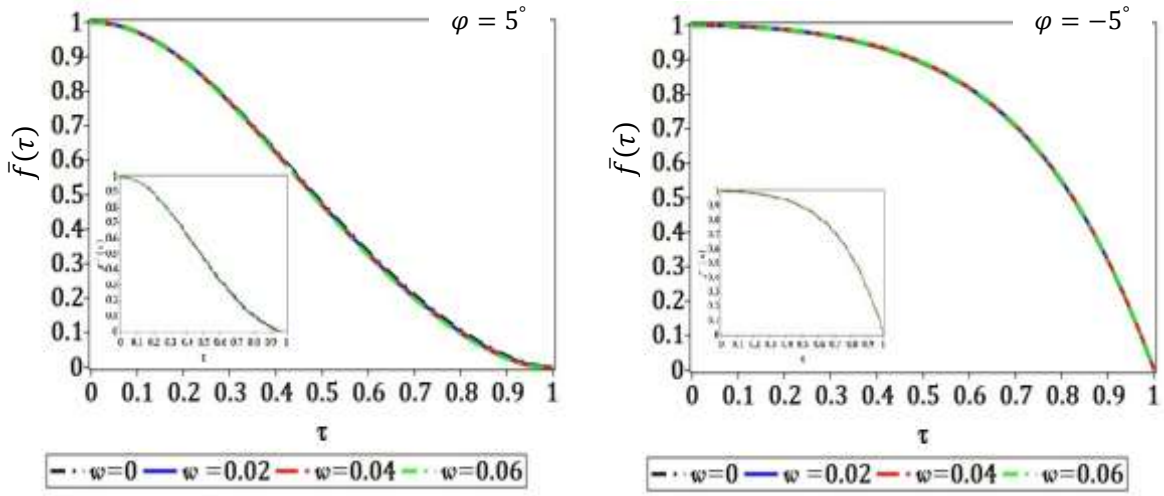

Fig. 8. w changed to Re = 100, Ha = 50 for TiO_2

Material Cu

Figure 9 displays the effect of the Hartmann number on the velocity profiles. From this figure note that the growing of Hartmann number lead to reduces the velocity profile for diverging and converging channels. Furthermore, by raising the Hartmann number in both channels, it is evident that there has been no backflow. The fluid velocity increases with the Reynolds number for the converging channel, while it occurs in the opposite direction for the divergent channel, as shown in Figure 10. Figure 11 illustrates the fluid velocity decreases as the nanofluid volume fraction increases for divergent channel, while in case convergent channel, the fluid velocity increases.

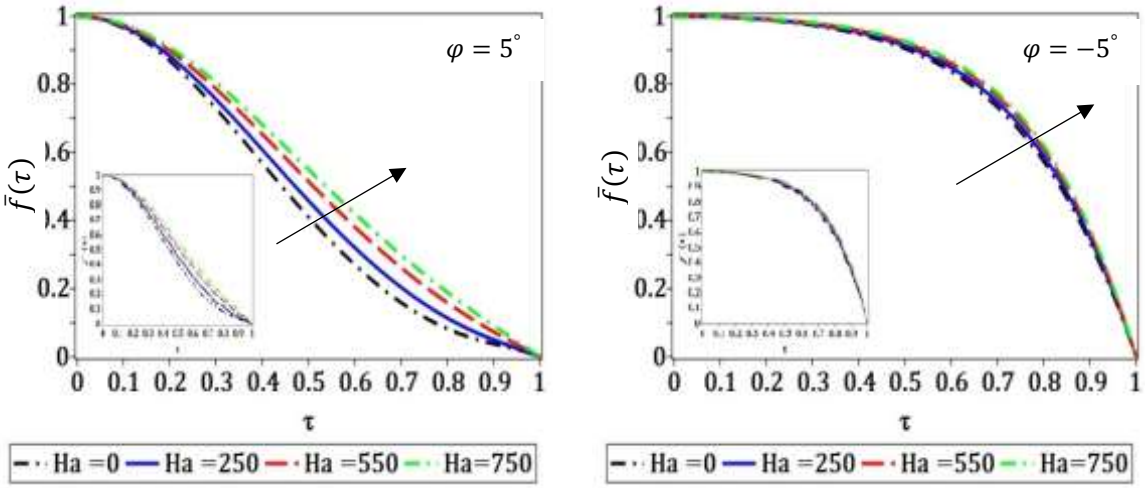

Fig. 9. Ha changed to Re $= 100, w = 0.05$ for Cu

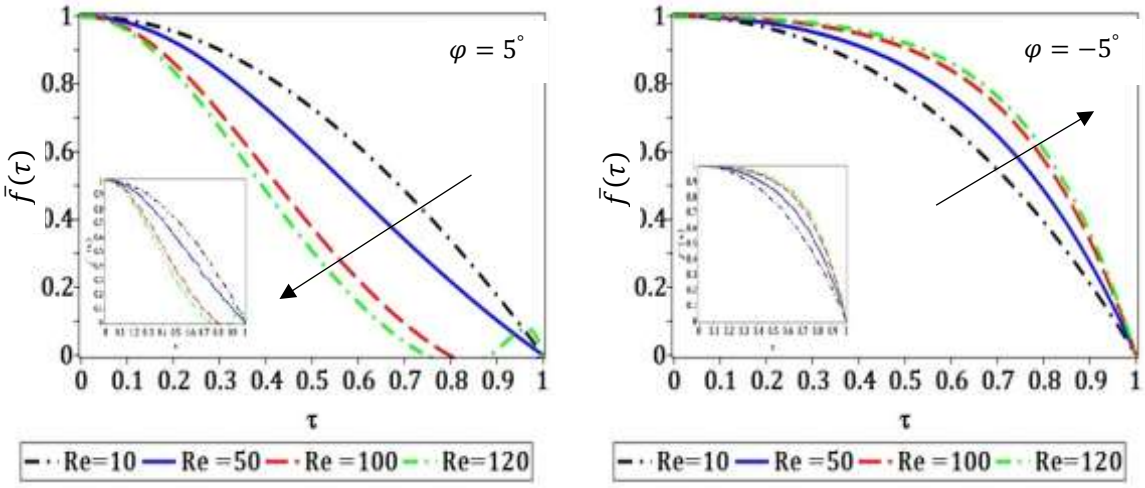

Fig. 10. Re changed to Ha $= 50, w = 0.05$ for Cu

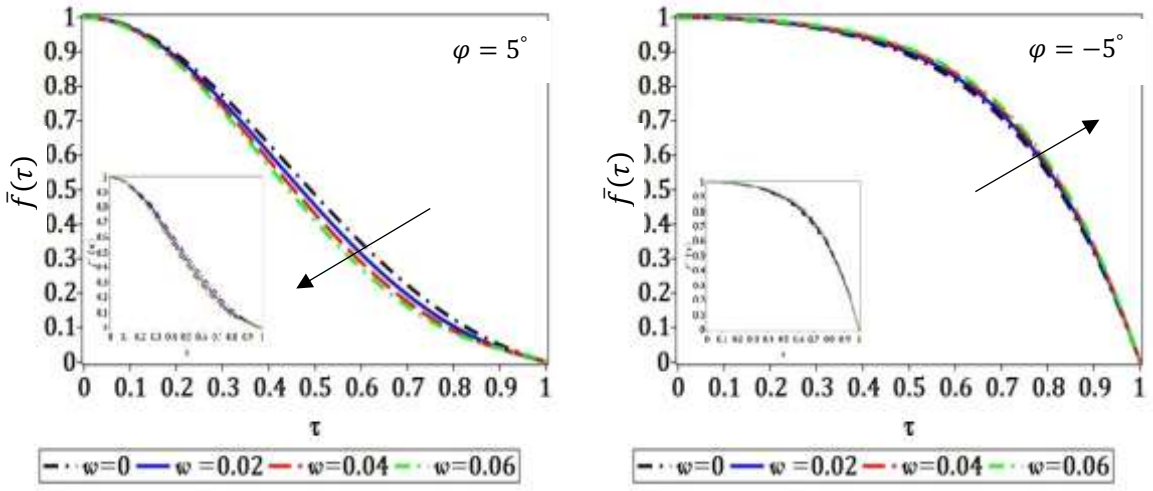

Fig. 11. w changed to Re = 100, Ha = 50 for Cu

Physically, the greater viscosity at the border causes resistance and, as a result, an increase in the momentum boundary layer, which is why the Reynolds number affects the velocity distribution. The relationship between velocity and nanofluid volume fraction is demonstrated, with a consistent decline in the velocity profile as the nanofluid volume fraction increases. The fluid is moved down the channel with no nanofluid volume percentage when $w = 0$ in this plot. The nanofluid volume fraction affects the fluid and reduces the thickness of the momentum barrier layer because of the large energy exchange rate that occurs when fluid molecules move through the nonparallel channel. The divergent-convergent plates response to channel opening angles. Open channel angles are relatively wide in order to stop fluid backflow. In the diverging channel, backflow is possible but not problematic in the converging channel. A high Reynolds number in the presence of strong magnetic field strength prevents back flow. As demonstrated, a significant decrease in the velocity profile is obtained through a quantitative increase in the channel angle. The intensity of the magnetic field and the decrease in fluid flow through the nonparallel channel indicate how the magnetic field affects flow. Plotting indicates that the absolute velocity drops. Physically speaking, this can be explained by the presence of resistive forces at the channel's edge due to an increase in boundary layer thickness, which retards the velocity field. The present study's objective is to look at.The improved analytical approach for magneto-hydrodynamic flow between two non-parallel walls. We aim to investigate the impact of the semi-angle formed by two walls on the velocity profile in this section. Additionally, we wish to verify the validity and correctness of the acquired findings compared to the numerical solution. Figure 3, Figure 4, Figure 6, Figure 7, Figure 9, Figure 10 and Figure 11 show the effect of semi-angle on the velocity profiles for diverging and converging channels. The velocity curves show that the wall transmission rate is more effective in the velocity profile for both convergent $\varphi < 0$ and divergent $\varphi > 0$ cases. As can be seen in Figure 5 and Figure 8, there are good agreements.

7. The Analysis of Convergence for q-HAM, LTC-q-HAM and ZTC-q-HAM

Here, the convergence of the analysis of the approximate analytical solution that outcome form implementation q-HAM, LTC-q-HAM and ZTC-q-HAM to solve the nonlinear ordinary differential equation. Also, the deriving and analyzing the convergence condition for testing these solutions in the following manner:

Definition 7.1: Let Λ be the Banach space, D a nonlinear mapping defined by $D: \Lambda \to \mathbb{R}$ and $\mathbb{R}$ is the real number. Then, the series of solutions of q-HAM, LTC-q-HAM and ZTC-q-HAM can be expressed in the following form

$$\bar{F}_i = \sum_{j=0}^{i} \bar{f}_j, \;\; i = 1,2,3,4, \ldots, \quad \bar{F}_{i+1} = \mathrm{D}(\bar{F}_i).$$

Definition 7.2: The nonlinear mapping T satisfies the Lipschitz condition for $\Pi \in R$ and,$0 < \Pi < 1$, yield

$$\|D(\bar{F}_{i+1}) - D(\bar{F}_i)\| \leq \Pi \|\bar{F}_{i+1} - \bar{F}_i\|.$$

Theorem 7.1.[11] The series of the approximate analytical solution $\bar{F} = \sum_{i=0}^{\infty} \bar{f}_i$ of q-HAM, q-HAM, LTC-q-HAM and ZTC-q-HAM is converges. If the condition is satisfied

$$\left\|\bar{F}_i - \bar{F}_j\right\| \to 0 \text{ as } j \to \infty, 0 < \Pi < 1,$$

To achieve convergence, from Definition (7.1), Definition (7.2) and Theorem (7.1) parameter values Π^i can be extracted by using the relationship below

$$\Pi^i = \begin{cases} \frac{\|\bar{F}_{i+1}\|}{\|\bar{F}_i\|}, & \|\bar{F}_i\| \neq 0, \\ 0, & \|\bar{F}_i\| = 0, \end{cases} \quad i = 0,1,2, \ldots$$

The areas convergence of the values parameters h are provided in Table 18 that shows the convergence values for this parameter. Furthermore, from Table 19 and Table 20 can be seen that the value of Π^i between 0 and 1. These tables indicate that the powers of Π found by applying ZTC-q-HAM and LTC-q-HAM convergence to zero faster than the powers of Π that were found based on q-HAM. Finally, we can say that ZTC-q-HAM and LTC-q-HAM represent a better convergence than q-HAM.

Table 18
The regions of the values h for $Ha = 0, Re = 10, \varphi = 3^{\circ}, w = 0.01$

M	Al_2O_3	TiO_2	Cu
1	$-1.1 \leq h \leq -1$	$-1.1 \leq h \leq -0.9$	$-1.1 \leq h \leq -0.9$
2	$-2.2 \leq h \leq -1.7$	$-2.2 \leq h \leq -1.8$	$-2.2 \leq h \leq -1.8$
3	$-3.3 \leq h \leq -2.7$	$-3.4 \leq h \leq -2.6$	$-3.2 \leq h \leq -2.6$
4	$-4.2 \leq h \leq -3.4$	$-4.4 \leq h \leq -3.4$	$-4.3 \leq h \leq -3.5$
5	$-5.4 \leq h \leq -4.3$	$-5.4 \leq h \leq -4.3$	$-5.5 \leq h \leq -4.3$
6	$-6.6 \leq h \leq -5.2$	$-6.5 \leq h \leq -5.2$	$-6.9 \leq h \leq -5.2$

Table 19
The values of Π for the L_∞-norm when $n = 1.5, h = -1.5, \hat{\rho}_s = 3970, Ha = 0, Re = 10, \varphi = 3^\circ, w = 0.01$

Π^i	q-HAM	ZTC-q-HAM	LTC-q-HAM
Π^0	0.06624371960	0.09174755180	0.06624371870
Π^1	0.00797892526	0.00797893373	0.00797892373
Π^2	0.00524494921	0.00524344513	0.00524344513
Π^3	0.00407958071	0.00004219893	0.00005495325
⋮	⋮	⋮	⋮

Table 20
The values of Π for the L_2- norm when $n = 1.5, h = -1.5, \hat{\rho}_s = 3970, Ha = 0, Re = 10, \varphi = 3^\circ, w = 0.01$

Π^i	q-HAM	ZTC-q-HAM	LTC-q-HAM
Π^0	0.04827327593	0.04827327541	0.04827327541
Π^1	0.00711729651	0.00711730469	0.00711729469
Π^2	0.00470190564	0.00470045003	0.00470045003
Π^3	0.00370704567	0.00004759753	0.00006198738
⋮	⋮	⋮	⋮

8. Conclusion

The magneto-hydrodynamic Jeffrey-Hamel nano-fluid flow with nanoparticles between two non-parallel plane walls for divergent and convergent channels was studied. The governing equations were transformed into nonlinear differential equation and resolved by q-homotopy analysis method. Also, the results solution of the q-homotopy analysis method was improved by the Laplace transform and the EL-Zaki transform through the intervention of the convolution theory. These solutions are more accurate than the solutions of the q-homotopy analysis method for selected values of the governing physical parameters. Consequently, it is close to the standard method to the numerical solution bvp4c. It can be said that the improved method is better than the standard method for solving non-linear ordinary differential equations. The improved method has high accuracy in solving nonlinear problems such as Jeffrey Hamel's flow nanofluid, and the results obtained were accurate by comparing them with the results of previous studies [7,9,18-20]. The increasing of the Hartmann number will not result in an increase in reverse flow at larger angles because an increase in the Reynolds number causes a decrease in the velocity profile and eliminates reverse flow in the converging channel. The importance of this study has a large and important role in many applications, especially in the fields of engineering, medical technologies, science, and natural processes.

References

[1] Khidir, Ahmed A. "A new spectral-homotopy perturbation method and its application to Jeffery-Hamel nanofluid flow with high magnetic field." *Journal of Computational Methods in Physics* 2013, no. 1 (2013): 939143. https://doi.org/10.1155/2013/939143

[2] Abdulridah, Saja I., and Abeer M. Jasim. "Semi-Analytical Assessment of Magneto-Hydrodynamic Nano-Fluid Flow Jeffrey-Hamel Problem." *Baghdad Science Journal* 21, no. 1 (2024): 0161-0161. https://doi.org/10.21123/bsj.2023.7955

[3] Jasim, Abeer Majeed. "New Analytical Study for Nanofluid between Two Non-Parallel Plane Walls (Jeffery-Hamel Flow)." *Journal of Applied and Computational Mechanics* 7, no. 1 (2021): 213-224.

[4] Jeffery, G. B. "The two-dimensional steady motion of a viscous fluid." *Russian Journal of Nonlinear Dynamics* 5, no. 1 (2009): 101-109. https://doi.org/10.20537/nd0901013

[5] Hamel, G., Bewgungen Spiralformige, and Flussigkeiten Zaher. "Dersdeutschen jahresbericht." *Math. Ver* 25 (1916): 34-60.

[6] Moghimi, S. M., Davood Domiri Ganji, H. Bararnia, M. Hosseini, and M. Jalaal. "Homotopy perturbation method for nonlinear MHD Jeffery-Hamel problem." *Computers & Mathematics with Applications* 61, no. 8 (2011): 2213-2216. https://doi.org/10.1016/j.camwa.2010.09.018
[7] Ganji, Z. Z., Davood Domiri Ganji, and Mehdi Esmaeilpour. "Study on nonlinear Jeffery-Hamel flow by He's semi-analytical methods and comparison with numerical results." *Computers & Mathematics with Applications* 58, no. 11-12 (2009): 2107-2116. https://doi.org/10.1016/j.camwa.2009.03.044
[8] Azimi, Mohammadreza, and Alireza Azimi. "Study on effect of semi-angle between non-parallel walls on magneto hydro dynamic Jeffery Hamel flow using semi-analytical approach." *Journal of Chemical Engineering and Materials* 4, no. 5 (2013): 67-71. https://doi.org/10.5897/JCEMS2013.0153
[9] Motsa, S. S., P. Sibanda, F. G. Awad, and S. Shateyi. "A new spectral-homotopy analysis method for the MHD Jeffery-Hamel problem." *Computers & Fluids* 39, no. 7 (2010): 1219-1225. https://doi.org/10.1016/j.compfluid.2010.03.004
[10] Hasan, Maysoon H., and Abdul-Sattar J Ali Al-Saif. "Applications of q-Homotopy analysis with Laplace Transform and Pade' approximate method for Solving Magneto Hydrodynamic boundary-layer equations." *Journal of Computational Applied Mechanics* 54, no. 2 (2023): 204-218.
[11] Akinyemi, Lanre, and Shaheed N. Huseen. "A powerful approach to study the new modified coupled Korteweg-de Vries system." *Mathematics and Computers in Simulation* 177 (2020): 556-567. https://doi.org/10.1016/j.matcom.2020.05.021
[12] Bhadane, Prem Kiran G., and V. H. Pradhan. "Elzaki transform homotopy perturbation method for solving gas dynamics equation." *International Journal of Research in Engineering and Technology* 2, no. 12 (2013): 260-264. https://doi.org/10.15623/ijret.2013.0212045
[13] Halil, A. N. A. Ç., Mehmet Merdan, and Tülay Kesemen. "Homotopy perturbation Elzaki transform method for obtaining the approximate solutions of the random partial differential equations." *Gazi University Journal of Science* (2022): 1-1.
[14] Bhadane, Prem Kiran G., and V. H. Pradhan. "Elzaki transform homotopy perturbation method for solving gas dynamics equation." *International Journal of Research in Engineering and Technology* 2, no. 12 (2013): 260-264. https://doi.org/10.15623/ijret.2013.0212045
[15] Moghimi, S. M., G. Domairry, Soheil Soleimani, E. Ghasemi, and H. Bararnia. "Application of homotopy analysis method to solve MHD Jeffery-Hamel flows in non-parallel walls." *Advances in Engineering Software* 42, no. 3 (2011): 108-113. https://doi.org/10.1016/j.advengsoft.2010.12.007
[16] Ganji, Davood Domiri, and Mohammadreza Azimi. "Application of DTM on MHD Jeffery Hamel problem with nanoparticle." *UPB Scientific Bulletin Series D* 75, no. 1 (2013): 223-230.
[17] El-Tawil, M. A., and S. N. Huseen. "The q-homotopy analysis method (q-HAM)." *International Journal of Applied Mathematics and Mechanics* 8, no. 15 (2012): 51-75.
[18] Esmaeilpour, Mehdi, and Davood Domiri Ganji. "Solution of the Jeffery-Hamel flow problem by optimal homotopy asymptotic method." *Computers & Mathematics with Applications* 59, no. 11 (2010): 3405-3411. https://doi.org/10.1016/j.camwa.2010.03.024
[19] Hamadiche, Mahmoud, Julian Scott, and Denis Jeandel. "Temporal stability of Jeffery-Hamel flow." *Journal of Fluid Mechanics* 268 (1994): 71-88. https://doi.org/10.1017/S0022112094001266
[20] Imani, A. A., Y. Rostamian, D. D. Ganji, and H. B. Rokni. "Analytical investigation of jeffery-hamel flow with high magnetic field and nano particle by RVIM." *Intnernational Journal of Engineering* 25, no. 3 (2012): 249-256. https://doi.org/10.5829/idosi.ije.2012.25.03c.09